

## Quantum properties of charged ferroelectric domain walls

B. Sturman,<sup>1</sup> E. Podivilov,<sup>1</sup> M. Stepanov,<sup>2</sup> A. Tagantsev,<sup>3</sup> and N. Setter<sup>3</sup>

<sup>1</sup>*Institute of Automation and Electrometry, Russian Academy of Sciences, 630090 Novosibirsk, Russia*

<sup>2</sup>*Department of Mathematics, University of Arizona, Tucson, Arizona 85721, USA*

<sup>3</sup>*Swiss Federal Institute of Technology (SPFL), CH-1015 Lausanne, Switzerland*

(Received 29 September 2015; revised manuscript received 18 November 2015; published 23 December 2015)

We consider the properties of charged domain walls in ferroelectrics as a quantum problem. This includes determination of self-consistent attracting 1D potential for compensating charge carriers, the number and positions of discrete energy levels in this potential, dependencies on the ferroelectric characteristics, as well as the spatial structure and formation energy of the wall. Our description is based on the Hartree and Thomas-Fermi methods and Landau theory for the ferroelectric transitions. Changeover from a few to many quantum levels (with the electron binding energies  $\sim 1$  eV) is controlled by a single characteristic parameter. The quantum models well describe the core of the wall, whose width is typically  $\sim 10$  nm. Additionally, the walls possess pronounced long-range tails which are due to trap recharging. For the trap concentration  $N_t = (10^{17}-10^{18}) \text{ cm}^{-3}$ , the tail length  $\ell$  is of the  $\mu\text{m}$  scale. On the distances much larger than  $\ell$  the walls are electrically uncoupled from each other and the crystal faces.

DOI: [10.1103/PhysRevB.92.214112](https://doi.org/10.1103/PhysRevB.92.214112)

PACS number(s): 77.80.Dj, 72.20.Jv

### I. INTRODUCTION

Interfaces between two distinct materials or material states are quasi-two-dimensional objects which display uniquely distorted electronic structures and ionic displacements. Properties of such interfaces can therefore be entirely different from those of the parent materials. Among the systems of this kind that have recently attracted the attention of researchers are heterointerfaces between metal oxides [1,2] and compositionally homogeneous interfaces such as ferroic domain walls [3–7].

The anomalous properties of the material modified by the presence of domain walls in ferroics are especially attractive for their variability. The walls can change positions, shapes, and thereby also intrinsic properties in a controlled way so that they can be used as a rearrangeable functional element [8].

The charged domain walls (CDWs), where the normal component of the spontaneous polarization shows a strong jump, are of special interest. It was believed for a long time that CDWs cannot exist in ferroelectrics because the electric fields of the bound polarization charge destabilize the system. Nevertheless, CDWs were occasionally documented in the past [9–13]. Their existence is due to a strong screening of the bound charge by free carriers. Owing to such screening, CDWs can serve as reconfigurable quasidopant [7], leading to the formation of a sheet of degenerate electronic gas with a local conductivity enhancement up to nine orders of magnitude [6]. This phenomenon justifies a growing interest to CDWs. Recently, they were identified and studied in many materials:  $\text{Pb}(\text{Zr},\text{Ti})\text{O}_3$  [4,14–16],  $\text{PbTiO}_3$  [17],  $\text{BaTiO}_3$  [6,18,19],  $\text{LiNbO}_3$  [20–22], improper ferroelectric manganites [5,23,24], hybrid improper ferroelectric  $(\text{Ca},\text{Sr})_3\text{Ti}_2\text{O}_7$  [25], and organic ferroelectrics [26].

On the theoretical side, the attention to CDWs was paid more 40 yr ago [27] with the prediction of the quasidopant effect. Later, an appreciable work was done on the properties of CDWs and the effects associated with them [28–34]. At the same time, no attention was paid to the quantum structure of CDWs which can actually be viewed as rearrangeable

quantum wells. Specifically, in all publications, the electronic gas at CDWs was treated either using the Thomas-Fermi approximation or the Boltzmann statistics, and the electron spectrum of the wall was missing from the considerations. Besides, recharging of localized states in the forbidden gap, typical of realistic ferroelectrics, was ignored. This led to nonvanishing electrostatic potential far from CDWs [30].

The goal of this paper is to fill the aforementioned gaps in the theoretical treatment of CDWs. Proceeded by general relations (Sec. II), the main results are presented in two subsequent sections.

In Sec. III we treat CDWs as multielectron 1D atoms within the Hartree and Thomas-Fermi methods [35]. This includes a self-consistent determination of the polarization profile  $P(z)$ , the electrostatic wall potential  $\varphi(z)$ , the electronic energy levels and wave functions in this potential, and the occupation numbers for the subbands caused by free transverse electron movement. The whole system is controlled by a single parameter  $Q$  combining the ferroelectric characteristics and the electron mass. For  $0 < Q \lesssim 3$ , there is one or a few energy levels, and the electron charge density  $\rho$  cannot be treated as a function of  $\varphi$ . With increasing  $Q$ , we have a quick changeover to the Thomas-Fermi physical pattern, where the number of levels is big and  $\rho = \rho(\varphi)$ . The binding energies of screening electrons are typically well above the thermal energy.

Section IV is devoted to the impact of localized states (traps) in the forbidden gap on the CDW properties. This impact, considered via the density of electronic states, is crucial: For an arbitrary position of the Fermi level  $E_F$  in the forbidden gap, the electrostatic potential  $\varphi$  decays outside CDW because of trap recharging. Without this process, the locality of CDWs is missing. For the trap concentration  $N_t \lesssim 10^{18} \text{ cm}^{-3}$ , the results of Sec. III well describe the core of the wall, whereas the localized states are responsible for pronounced long-range tails. For  $N_t > 10^{19} \text{ cm}^{-3}$ , the whole charge screening is due the localized electrons. Also we show a strong impact of the localized states on the wall energies. This issue includes generalization of the known thermodynamic relations for dielectrics [36].

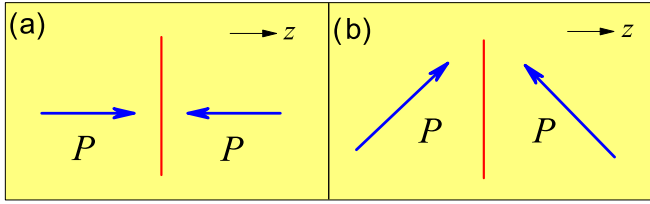


FIG. 1. (Color online) Geometrical schemes for positively charged head-to-head 180° (a) and 90° (b) domain walls. For negatively charged tail-to-tail walls the vectors  $\mathbf{P}$  have to be inverted. The longitudinal  $z$  axis is perpendicular to the wall plane  $x, y$ .

The results of the paper, including estimates for experimentally valuable situations, are summarized in Sec. V.

## II. GENERAL RELATIONS AND ASSUMPTIONS

Our subsequent considerations are relevant to the cases of 180° and 90° CDWs depicted in Fig. 1. The walls can be of the head-to-head or tail-to-tail type. In both cases the problem is one-dimensional (1D); all polarization components depend only on the longitudinal (across the wall) coordinate  $z$ . The basic case for us is 180° walls. The results for 90° walls can be obtained by a renormalization procedure; see below.

Let  $P_z \equiv P = P(z)$ ,  $\varphi = \varphi(z)$ , and  $\rho = \rho(z)$  be the spontaneous polarization, the electrostatic potential, and the bulk charge density of the compensating carriers. The functions  $\varphi(z)$  and  $\rho(z)$  tend to zero for  $|z| \rightarrow \infty$ . Without loss of generality we consider the head-to-head configuration when the bound polarization charge is positive and the compensating charge carriers are electrons. Here we have  $P(z) \rightarrow \pm P_0$ , for  $z \rightarrow \mp\infty$ , where  $P_0 > 0$  is the value of spontaneous polarization in the absence of electric fields. Correspondingly, the total bound charge is  $2P_0$ ; it has the dimension of surface charge density.

According to Landau theory of the second-order ferroelectric transitions, the electrostatic field  $-d\varphi/dz$  is linked to  $P$  by the equation of state [28,36],

$$-\frac{d\varphi}{dz} = \alpha P + \beta P^3, \quad (1)$$

where  $\alpha < 0$  and  $\beta > 0$  in the ferroelectric state. The quantity  $\varepsilon_f = 2\pi/|\alpha|$  is the contribution of the ferroelectric subsystem to the dielectric permittivity. Smallness of  $|\alpha|$  ensures large values of  $\varepsilon_f$ . According to Eq. (1),  $P_0 = \sqrt{|\alpha|/\beta}$ . For the temperature  $T$  close to the Curie temperature  $T_c$  we have  $\alpha \propto |T - T_c|$  and  $P_0 \propto |T - T_c|^{1/2}$ .

Often, an additional ‘‘correlation’’ term  $-\kappa d^2P/dz^2$  is present on the right-hand side of Eq. (1). It provides the wall thickness  $\sim \sqrt{\kappa/|\alpha|}$  and is important for neutral domain walls. For CDWs, strong electron screening prevents such fast polarization changes, so that, similar to [28], we disregard this term.

The second basic equation follows from the general relation of electrostatics  $dD/dz = 4\pi\rho$ , where  $D = -\varepsilon_b d\varphi/dz + 4\pi P$  is the electric displacement and  $\varepsilon_b$  is the background dielectric permittivity. Owing to the smallness of  $\varepsilon_b/\varepsilon_f = \alpha\varepsilon_b/2\pi$ , the first term in the expression for  $D$  is negligible,

and we have with a good accuracy

$$\frac{dP}{dz} = \rho. \quad (2)$$

If the charge density  $\rho$  is a function of  $\varphi$ , Eqs. (1) and (2) form a closed set of ordinary differential equations. Using this set and the boundary conditions  $\varphi(\infty) = 0$  and  $P^2(\infty) = P_0^2$ , one can check the conservation law

$$\frac{|\alpha|P_0^2}{4} \left(1 - \frac{P^2}{P_0^2}\right)^2 + \int_0^\varphi \rho(\varphi') d\varphi' = 0. \quad (3)$$

This relation allows one to express  $\varphi$  by  $P$  (or vice versa) for any particular dependence  $\rho(\varphi)$  and obtain a first-order differential equation for  $P$  or  $\varphi$ .

Generally, the charge density  $\rho$  cannot be treated as a function of  $\varphi$ . In the general case,  $\rho(z)$  is expressed by the wave functions of electrons, and the latter obey the Schrödinger equation in the self-consistent potential  $\varphi(z)$ . Equations (1) and (2) do not form here a closed set. However, under certain restrictions on the crystal parameters, when the number of contributing wave functions is big enough, the charge density can be approximated by a function  $\rho(\varphi)$  with a good accuracy.

Last, we consider in some detail what happens when changing to the case of 90° CDWs [see Fig. 1(b)], as applied to the tetragonal phase of BaTiO<sub>3</sub> crystals. The equation of state (1) can be generalized here to include the transverse polarization component. It is shown [37] that this component can be expressed by  $P \equiv P_z$ , so that we return to the 1D equation of state Eq. (1) with some effective coefficients  $\alpha$  and  $\beta$ . Thus, our theory is applicable also to the case of 90° CDWs. A specific feature of BaTiO<sub>3</sub> crystals is that the effective coefficients  $\alpha$  and  $\beta$  are anomalously small, owing to the large anisotropy of the dielectric susceptibility [37].

## III. CDWs AS 1D ATOMS

### A. Formulation of quantum problem

Generally, the multielectron quantum problems are extremely complicated. The simplest theoretical tools for them, which are widely used in physics, are the Hartree and Thomas-Fermi methods [35]. They account for self-consistent electron potential, but neglect the exchange interaction and the correlation effects. Usually, it is sufficient to reproduce the main physical tendencies. More accurate Hartree-Fock and density-functional methods [38] are much more complicated. Below we restrict ourselves to the above two simplest methods.

Let  $\Psi_j = \Psi_j(z)$  be the electron wave function for the energy level  $E_j$  ( $j = 0, 1, \dots$ ) in the electrostatic potential  $\varphi(z)$ . This function describes a finite electron movement in the longitudinal  $z$  direction, so that  $\Psi_j(z) \rightarrow 0$  for  $z \rightarrow \pm\infty$ . In the 1D case, the functions  $\Psi_j(z)$  can be treated as real quantities; they are normalized such that  $\int_{-\infty}^{\infty} \Psi_j^2(z) dz = 1$ . The potential energy for electrons is  $-e\varphi$ , where  $e > 0$  is the elementary charge. Within the Hartree method, the wave functions  $\Psi_j(z)$  obey the Schrödinger equation [35],

$$\frac{d^2\Psi_j}{dz^2} = -\frac{2m_e}{\hbar^2}(e\varphi + E_j)\Psi_j, \quad (4)$$

where  $m_e$  is the effective electron mass.

The total wave functions for  $j$ th level must account also for free electron movement in the transverse  $x, y$  directions. They are given by the product  $\Psi_j(z)\Psi_{\mathbf{k}}(\mathbf{r})$ , where  $\mathbf{r} = (x, y)$  and  $\mathbf{k} = (k_x, k_y)$  is the transverse wave vector. Employing the  $L$  periodic in  $x, y$  boundary conditions and the plane-wave approximation, we have  $\Psi_{\mathbf{k}}(\mathbf{r}) = (1/L)\exp(i\mathbf{k} \cdot \mathbf{r})$ , where  $k_{x,y} = 2\pi n_{x,y}/L, n_{x,y}$  are independent integers, and  $\int |\Psi_{\mathbf{k}}(\mathbf{r})|^2 d\mathbf{r} = 1$ . Owing to the transverse movement, the total electron energy in the  $j$ th subband is  $E_j + k^2\hbar^2/2m_e$ .

Each quantum state  $(j, \mathbf{k})$  can be occupied by no more than two electrons with opposite spins. The total number of electrons in the subband  $j$ , divided by the transverse cross section  $L^2$ , we denote  $N_j$ . Correspondingly, the bulk charge density of electrons is

$$\rho = -e \sum_j N_j \Psi_j^2, \quad (5)$$

and the sum  $N = \sum_j N_j$  is the total density of electrons per unit surface element. Since the charge compensation for CDWs must be almost total to prevent destabilization of the system, we have  $N = 2P_0/e$  with a high accuracy.

Generally, the choice of the occupation numbers  $N_j$  is restricted only by the sum condition  $\sum_j N_j = 2P_0/e$ . This corresponds to arbitrary excited states of our multielectron system. However, for the ground state of our multielectron system, possessing the lowest energy, strong additional constraints on  $N_j$  have to be imposed. It is evident that each subband  $j$  has to be filled up to the same boundary electron energy  $E_B$ . This quantity is analogous to the maximum energy of bound electrons in multielectron atoms. Transferring from summation to integration over  $\mathbf{k}$ , we have  $N_j = 2 \int_{s_j} dk_x dk_y / (2\pi)^2$ , where 2 is the spin factor and  $s_j$  is a 2D sphere of the radius  $k_j^2 = 2m_e(E_B - E_j)/\hbar^2$ . Performing the integration in the polar coordinate system, we get

$$N_j = \frac{m_e}{\pi \hbar^2} (E_B - E_j). \quad (6)$$

Substituting  $N_j$  into the relation  $\sum_j N_j = N$ , we obtain

$$\sum_{j=0}^{j_{\max}} E_j = sE_B - \pi \hbar^2 N / m_e, \quad (7)$$

where  $s = j_{\max} + 1$  is the total number of levels (subbands). Thus, the boundary electron energy  $E_B$  is expressed by  $N = 2P_0/e$  and the sum of  $E_j$ .

Now it is easy to see that Eqs. (1), (2), and (4) to (7), supplemented by the normalization condition for  $\Psi_j(z)$ , form a closed system for determination of  $\Psi_j, E_j, E_B, P, \rho, \varphi$ , and  $N_j$ . This system combines quantum behavior of electrons with classical behavior of  $P$  and  $\varphi$ . Within this description scheme, the charge density  $\rho$  is certainly not a function of  $\varphi$ .

The above closed set of equations can be substantially simplified after a proper normalization. To make it, we introduce the length parameter

$$d = (2\hbar^2/m_e e |\alpha| P_0)^{1/3} \quad (8)$$

and the dimensionless quantities of the coordinate  $\zeta$ , the polarization  $p$ , the wave functions  $\psi_j$ , the potential  $u$ , and

the energies  $\mathcal{E}_j$  and  $\mathcal{E}_B$ :

$$\begin{aligned} \zeta &= z/d, \quad p = P/P_0, \quad \psi = \sqrt{d} \Psi, \\ u &= -m_e d^2 e \varphi / \hbar^2, \quad \mathcal{E}_{j,B} = m_e d^2 E_{j,B} / \hbar^2. \end{aligned} \quad (9)$$

After this normalization, we have

$$\begin{aligned} \frac{dp}{d\zeta} &= -2 \sum_j \frac{N_j}{N} \psi_j^2, \\ \frac{d^2 \psi_j}{d\zeta^2} &= 2(u - \mathcal{E}_j) \psi_j, \\ \frac{du}{d\zeta} &= -2p(1 - p^2). \end{aligned} \quad (10)$$

Owing to Eqs. (6) and (7), this set includes the only external variable parameter  $N$ . The boundary conditions read  $u(\pm\infty) = \psi(\pm\infty) = 0$  and  $p(\pm\infty) = \mp 1$ . Obviously, the profiles  $u(\zeta)$  and  $p(\zeta)$  must be even and odd, respectively. As concern the wave functions  $\psi_j(\zeta)$ , they must be either even or odd. Last, we indicate that set (10) possesses the conservation law

$$p^2 - \frac{p^4}{2} + \sum_j \frac{N_j}{N} \left( \frac{d\psi_j}{d\zeta} \right)^2 - 2 \sum_j (u - \mathcal{E}_j) \frac{N_j}{N} \psi_j^2 = \frac{1}{2}. \quad (11)$$

The above properties simplify the subsequent analysis. In particular, it can be restricted to the range  $0 \leq \zeta < \infty$ .

Next we have to normalize Eq. (6). Using Eqs. (8) and (9), we rewrite it in the form

$$\frac{N_j}{N} = \frac{2}{Q} (\mathcal{E}_B - \mathcal{E}_j), \quad (12)$$

where

$$Q = \frac{4\pi P_0 d^2}{e} \equiv \frac{4\pi P_0^{1/3}}{e^{5/3}} \left( \frac{2\hbar^2}{|\alpha| m_e} \right)^{2/3} \quad (13)$$

is the only variable dimensionless parameter of our quantum problem. As we will see, this parameter characterizes the depth of the potential well and the number of localized levels  $s$ . In the terms of  $Q$ , Eq. (7) simplifies to

$$\sum_j \mathcal{E}_j = s\mathcal{E}_B - Q/2. \quad (14)$$

Using Eqs. (12) and (14), one can express explicitly the ratio  $N_j/N$  in set (10) by  $\{\mathcal{E}_j\}$  and  $Q$ .

Let us make numerical estimates. Here and later on we use the input material parameters

$$P_0 = 30 \mu\text{C}/\text{cm}^2, \quad |\alpha| = 10^{-2}, \quad m_e = 0.2m_0, \quad (15)$$

where  $m_0$  is the naked electron mass. The chosen values of  $P_0$  and  $|\alpha|$  are representative for perovskites. The effective masses are badly known for ferroelectrics, but it is known that  $m_e$  is often noticeably smaller than  $m_0$  in semiconductors. For the chosen parameters we have  $d \approx 2 \text{ nm}$ ,  $Q \approx 10^2$ , and  $N \approx 4 \times 10^{14} \text{ cm}^{-2}$ . Substantially smaller values of  $Q$  can be obtained for larger values of  $|\alpha|$  and  $m_e$  and smaller values of  $P_0$ .

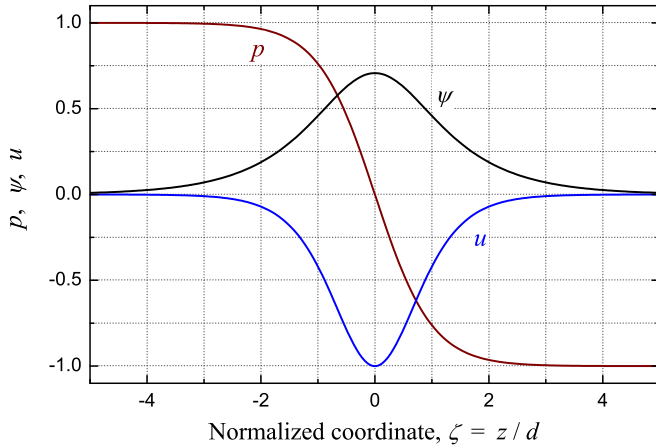


FIG. 2. (Color online) Ground-state screening. The spatial profiles of the normalized polarization  $p$ , wave function  $\psi$ , and potential  $u$  according to Eqs. (16).

## B. CDWs for Hartree screening

### 1. Ground-state screening

Let us assume that CDW possesses a single localized level  $E_0$ . In this case, one can check that Eqs. (10) admit the following solitonlike solution:

$$p = -\text{th}\zeta, \quad u = -\frac{1}{\text{ch}^2\zeta}, \quad \psi = \frac{1}{\sqrt{2}\text{ch}\zeta}, \quad \mathcal{E}_0 = -\frac{1}{2}. \quad (16)$$

It is illustrated by Fig. 2. All necessary conditions are fulfilled. The width of the domain wall  $w$ , determined as the distance between the points with  $p = \pm 1/2$ , is  $w \simeq d \ln 3 \simeq 1.1d$ . The width of the potential profile is slightly larger than  $d$ .

Next we obtain from Eq. (14) for the normalized boundary electron energy:  $\mathcal{E}_B = -(1 - Q)/2$ . It grows linearly with  $Q$  starting from the ground-state energy  $-1/2$ . Since  $\mathcal{E}_B$  cannot be positive, the ground-state screening is restricted to the region  $0 < Q \leq 1$ . For  $Q > 1$  the number of levels  $s$  must exceed 1.

It is worthy of mentioning that the potential  $-u_0/\text{ch}^2\zeta$  admits full investigation of discrete energy levels [35]. The actual value  $u_0 = 1$  is the boundary one between the cases of one and two levels.

### 2. Several localized levels

For the number of levels  $s > 1$ , we rely on numerical treatment of Eqs. (10). Solutions of these equations were found by the fixed-point iteration method. In each iteration we calculate a new potential  $u_{\text{new}}(\zeta)$  from an old one  $u_{\text{old}}(\zeta)$ , employing the following procedure. First, using the second equation of the set, we find the localized states  $\psi_j(\zeta)$  with their occupations  $N_j$  according to Eqs. (12) and (14). From these, using the first equation, we find  $P(\zeta)$ . Then the new potential  $u_{\text{new}}(\zeta)$  is found from the third equation. For better convergence the iterations  $u_{\text{old}} \rightarrow u_{\text{new}}$  are damped, the result of an iteration is  $(1 - c)u_{\text{old}} + cu_{\text{new}}$ , with  $0 < c \leq 1$ . Without damping the iterations could be not converging. A typical value of  $c$  was 0.1; near the threshold values of  $Q$  (see below) we

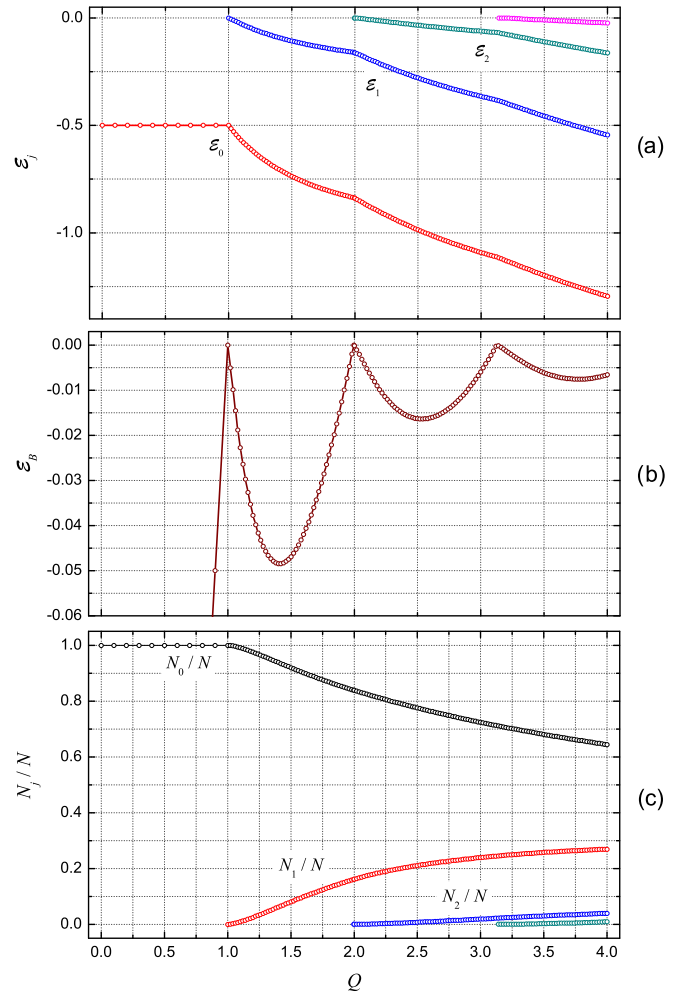


FIG. 3. (Color online) The normalized energies  $\mathcal{E}_j$ , the boundary electron energy  $\mathcal{E}_B$ , and the ratios  $N_j/N$  versus parameter  $Q$ .

used smaller values like 0.01 or even 0.001. The conservation law (11) was fulfilled with a high accuracy.

Dependencies of the normalized energies  $\mathcal{E}_j$ , of the normalized boundary energy  $\mathcal{E}_B$ , and of the ratios  $N_j/N$  on  $Q$  are presented in Fig. 3. The quantities  $\mathcal{E}_0$  and  $N_0/N$  stay constant up to the first threshold,  $0 < Q \leq Q_1^{\text{th}} = 1$ . At  $Q = 1$  the localized level 1 appears and the energy  $\mathcal{E}_1(Q)$  decreases starting from zero with a finite initial slope. Both functions  $\mathcal{E}_0(Q)$  and  $\mathcal{E}_B(Q)$  experience pronounced breaks of the first derivative at  $Q_1^{\text{th}}$ , the energy  $\mathcal{E}_B$  becomes negative again, while the ratio  $N_1/N$  grows quadratically from zero for  $Q - Q_1^{\text{th}} > 0$ . Similar, but much less pronounced, breaks of derivatives for  $\mathcal{E}_j(Q)$  and  $\mathcal{E}_B(Q)$  occur at each new threshold  $Q_{2,3,\dots}^{\text{th}}$ . The boundary electron energy stays negative and shows decreasing oscillations near zero. The decreasing ratio  $N_0/N$  exceeds substantially the ratios  $N_{1,2,3}/N$  in the whole shown range of  $Q$ , while the ground-state energy  $\mathcal{E}_0$  is well separated from the higher normalized energies.

As expected, the wave functions  $\psi_j(\zeta)$  are even for  $j = 0, 2, \dots$  and odd for  $j = 1, 3, \dots$ . The smaller  $|\mathcal{E}_j|$ , the weaker is the localization of  $\psi_j(\zeta)$ . For  $Q > 1$ , the profile  $u(\zeta)$  possesses a  $1/\text{ch}^2(\zeta)$ -like core and a relatively long tail related to the states with smallest energies  $\mathcal{E}_j$ . The widths of the

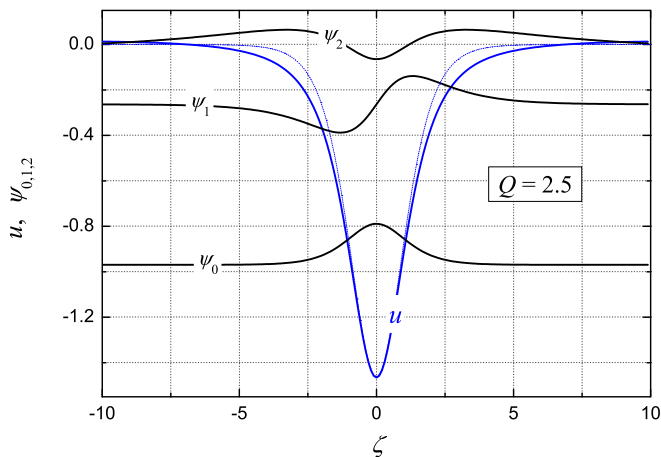


FIG. 4. (Color online) The normalized potential  $u(\zeta)$  and the wave functions  $\psi_{0,1,2}(\zeta)$  for  $Q = 2.5$ . The limiting values of the wave functions for  $|\zeta| \rightarrow \infty$  correspond to the energies  $\mathcal{E}_{0,1,2}$ . The dotted line gives a  $1/\text{ch}^2(\zeta)$ -like fit for  $u(\zeta)$ .

profiles  $p(\zeta)$  and  $u(\zeta)$  grow gradually with increasing  $Q$ ; see also below. The mentioned properties of  $u(\zeta)$  and  $\psi_j(\zeta)$  are illustrated by Fig. 4 for  $Q = 2.5$ .

Consider numerical estimates for the above quantum cases. The values  $Q \sim 1$  require much larger values of  $|\alpha|$  and smaller values of  $P_0$  compared to those given by Eq. (15) and representative for perovskites. Setting, e.g.,  $\alpha = 1/2$ ,  $m_e = m_0$ , and  $P_0 = 2 \mu\text{C}/\text{cm}^2$ , we obtain  $Q \approx 2$ , the wall width  $w \approx 1.3$  nm, and the binding energy  $|E_0| \approx 0.04$  eV. The conditions of validity of our theory, as formulated in Sec. II, are fulfilled.

### C. Thomas-Fermi screening

The case of many discrete levels,  $Q \gg 1$ , can be described within the Thomas-Fermi (TF) quasiclassical method [35]. Here the compensating charge density  $\rho$  is directly expressed by the electrostatic potential  $\varphi$ ,

$$\rho = -\frac{e(2m_e e\varphi)^{3/2}}{3\pi^2 \hbar^3}, \quad (17)$$

and  $\varphi > 0$  for head-to-head domain walls. Substituting this value into Eq. (3) and transferring to the normalized variables  $u$ ,  $p$ , and  $\zeta$  given by Eqs. (9), we get

$$u = -c_1 Q^{2/5} (1 - p^2)^{4/5}, \quad \frac{dp}{d\zeta} = -\frac{c_2}{Q^{2/5}} (1 - p^2)^{6/5}, \quad (18)$$

where  $c_1 = (15\pi/32\sqrt{2})^{2/5} \simeq 1.016$  and  $c_2 = 8\sqrt{2} c_1^{3/2}/3\pi \simeq 1.23$ . Despite the different quantum approach, the only dimensionless variable parameter in Eqs. (18) is again  $Q$ .

Now the functions  $p(\zeta)$  and  $u(\zeta)$  can be found readily. Setting  $p = -\text{th} f$ , we have  $u = -c_1 Q^{2/5}/\text{ch}^{8/5} f$ , and  $f$  is expressed by  $\zeta$  from the relation

$$c_2 \zeta / Q^{2/5} = \int_0^f \text{ch}^{2/5} x dx. \quad (19)$$

The scaling properties in  $Q$  are obvious.

The solid lines in Fig. 5 exhibit the shapes of the polarization and the potential; these shape functions are applicable to

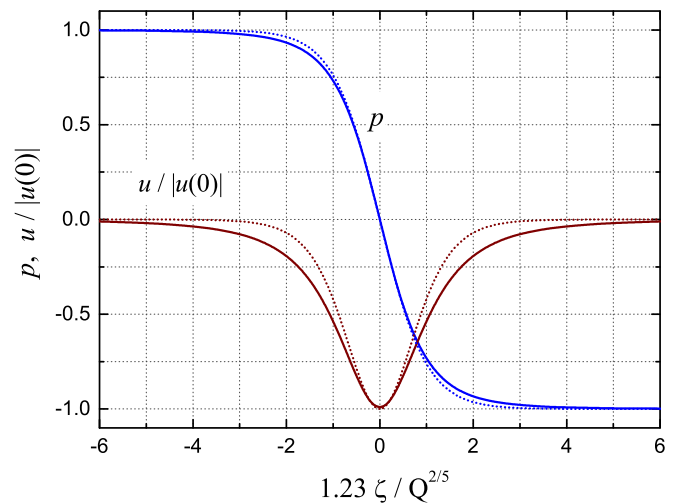


FIG. 5. (Color online) Thomas-Fermi dependencies  $p(\zeta)$  and  $u(\zeta)$  (the solid lines). The dotted lines show fitting functions  $\text{th}(1.23\zeta/Q^{2/5})$  and  $-1/\text{ch}^2(1.23\zeta/Q^{2/5})$ .

any  $Q$ . The dotted lines correspond to the fitting functions  $\text{th}(1.23\zeta/Q)$  and  $-1/\text{ch}^2(1.23\zeta/Q)$  inherent in the single-level Hartree case. One sees a noticeable broadening (with pronounced tails) of the potential profile compared to the fit.

Now we proceed to physical consequences of the above general TF relations.

The energy of the ground state  $E_0$  is an important characteristic. Since our case is quasiclassical, it is close to  $e\varphi(0)$ . The latter can be found from the above normalization relation for  $u(\zeta)$  and the relation  $u(0) = -c_1 Q^{2/5}$  that follows from Eq. (18). Thus, we arrive at an important relation for the binding energy of screening electrons:

$$|E_0| \simeq |e\varphi(0)| \simeq (2\pi|\alpha|P_0^2)^{2/5} \times (\hbar^2/m_e)^{3/5}. \quad (20)$$

For parameters (15) we have  $|E_0| \approx 0.6$  eV. With realistic values of  $P_0$ ,  $\alpha$ , and  $m_e$ , the binding energies  $\sim 1$  eV are available. Such energies strongly exceed the room-temperature thermal energy  $k_B T$ . Correspondingly, the temperature effects, like the Debye screening, are weak. At the same time, we have  $|E_0| \propto |T - T_c|^{4/5} \rightarrow 0$  and  $Q \propto |T - T_c|^{-1/2} \rightarrow \infty$  for  $T \rightarrow T_c$ . Thus, the potential well for electrons becomes very broad and shallow in the close vicinity of the Curie point.

The case of  $90^\circ$  CDWs in trigonal  $\text{BaTiO}_3$  crystals [6,30] requires an additional remark. Our estimate  $P_0 = 30 \mu\text{C}/\text{cm}^2$  is valid here, but the value of  $|\alpha|$  is smaller compared to the used one by a factor of  $\approx 15$  [37]. This leads to an additional factor of  $\approx 1/4$  in the estimate of  $|E_0|$ . This binding energy is still well above  $k_B T$ .

Since the function  $p(\zeta)$  is known, we can determine the width of the domain wall  $w$ . It is given by

$$w \simeq 0.91 \times d Q^{2/5} \quad (21)$$

and grows as  $Q^{2/5}$  with increasing  $Q$ . Using Eqs. (17) and (20), it is not difficult to express by  $w$  the maximum concentration of compensating electrons in the wall,  $|\rho(0)|/e \approx 2P_0/ew$ . For  $P_0 = 30 \mu\text{C}/\text{cm}^2$  and  $w = 10$  nm, we have  $|\rho(0)|/e \approx 4 \times 10^{20} \text{ cm}^{-3}$ . It should be noted that the above solution for

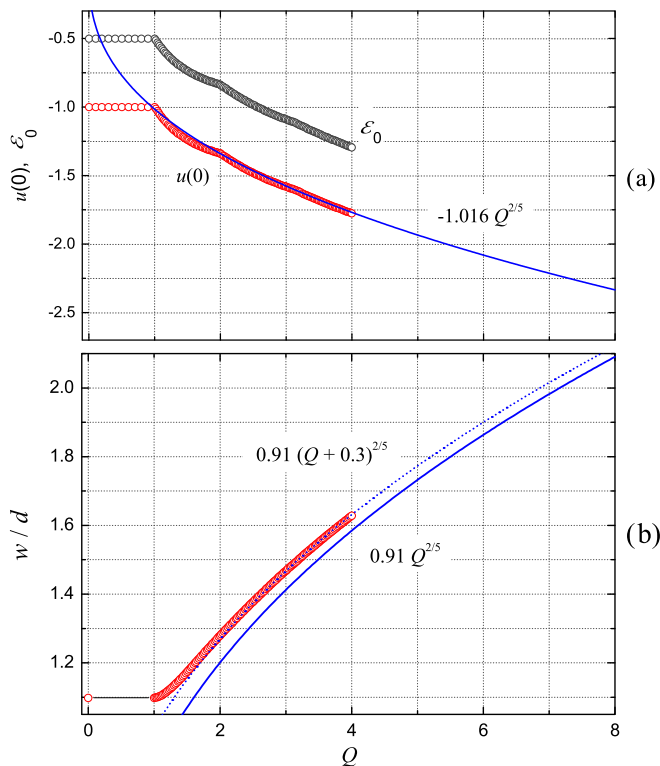


FIG. 6. (Color online) Crossover from Hartree to the TF case with increasing  $Q$ . The circles indicate the values calculated numerically from Eqs. (10), while the solid lines correspond to the TF method. (a) The data for  $u(0)$  and  $\mathcal{E}_0$ . (b) The data for the normalized wall width  $w/d$ ; the dotted line is a fit.

$P(z)$  and the estimates of  $w$  and  $|\rho(0)|/e$  differ from the corresponding relations of [28] only by notation.

Next we estimate the number of discrete energy levels in the potential  $-e\varphi(z)$  using the quasiclassical approach of [35]. It is given by  $s \approx Q^{3/5}$ , which corresponds to  $s \approx 15$  for  $Q \approx 10^2$ . Discreteness of the energy spectrum is thus well pronounced for CDWs. Also, it is useful to estimate the ratio  $E_1/E_0$  characterizing the position of the second energy level. With our potential profile  $u(\zeta)$ , we have found numerically that this ratio does not exceed  $1/2$  for  $Q \lesssim 10^2$ . Thus, the second level is well separated from the ground one. Since the momentum dependence of the electron energy ( $k^2 \hbar^2 / 2m_e$ ) is the same in all subbands, the mentioned properties may have clear manifestations for IR light-induced transitions.

The above results on the wall properties can be easily transferred to the case of tail-to-tail walls, where the screening species are holes. It is sufficient to replace  $m_e$  by the hole mass  $m_h$  in the relevant expressions.

Finally, we consider an important issue about crossover from the Hartree to the TF physical pattern with increasing  $Q$ . This crossover is expected for sufficiently large  $Q$ , but details are far from obvious. To quantify them, we superimpose the  $Q$  dependencies of the main wall characteristics obtained numerically and analytically for the Hartree and TF screening, respectively.

The solid line in Fig. 6(a) shows the TF dependence of  $u(0)$ , while the circles correspond to the Hartree values of  $u(0)$  and  $\mathcal{E}_0$ . One sees an *excellent and fast convergence* to the TF case

with increasing  $Q$ . In essence, the TF results for  $u(0)$  become valid already for  $Q \gtrsim 3$ . The same is valid for the boundary electron energy  $\mathcal{E}_B$ : It is about zero within the TF method and it is very close to zero for  $Q \gtrsim 3$  according to Fig. 3(b). The solid line in Fig. 6(b) gives the TF dependence of the normalized wall width  $w/d$  according to Eq. (21), while the circles give the numerical Hartree dependence. The relative difference becomes small for  $Q \gtrsim 3$ . Note that a slightly improved fitting function  $0.91(Q+0.3)^{2/5}$  gives an almost perfect agreement already for  $Q > 2$ .

Also, it is possible to compare the shapes of  $u(\zeta)$  calculated numerically and analytically for  $Q \leq 4$  within the Hartree and TF methods, respectively. For  $Q > 3$  they coincide practically within the line thickness.

Thus, the crossover to the TF screening occurs very fast and there is no gap in  $Q$  between the Hartree and TF physical patterns.

#### IV. IMPACT OF LOCALIZED ELECTRONS

Above we treated the CDWs as 1D atoms where the necessary amount of compensating electrons was granted. What happens when such a 1D atom is embedded into a real crystal matrix? The answer greatly depends on the electronic properties of this matrix.

It is well known that, in addition to delocalized band electrons, localized charge carriers populating the energy levels in the forbidden gap are present in any real dielectric or semiconductive material. Moreover, the localized states determine the position of the Fermi level in the forbidden gap. In wide-band-gap ferroelectrics, the concentration of the localized electrons is roughly of the order of  $10^{17} \text{ cm}^{-3}$  [39]. In doped ferroelectrics, it can reach  $10^{20} \text{ cm}^{-3}$ . Spatial redistribution of electrons over populated and empty localized states (trap recharging) contributes to the charge screening processes.

The effect of trap recharging on CDW properties was ignored so far. This led to distinct physical peculiarities: The electrostatic potential did not vanish far away from CDWs, so that any wall was coupled either to the sample faces or to neighboring walls (for periodic structures). In other words, CDWs were not local physical objects. We show below that account for trap recharging yields CDW locality and modifies the estimates of the wall energy. In what follows we restrict ourselves to the most important quasiclassical case where the compensating charge density can be treated as a function of the electrostatic potential,  $\rho = \rho(\varphi)$ .

##### A. Formalism of the density of electronic states

The electronic properties of material can be described by the energy density of electronic states  $\mathcal{N}(E)$  taken at  $\varphi = 0$ . This is a general characteristic of solid-state physics incorporating uniformly both the localized (trapped) and delocalized (band) electrons [40]. Being integrated over the energies  $-\infty < E \leq E_F$ , it gives the spatially homogeneous initial distribution of electrons in the low-temperature range. Owing to the charge neutrality of the medium, the corresponding negative electronic charge density is compensated by the positive background.

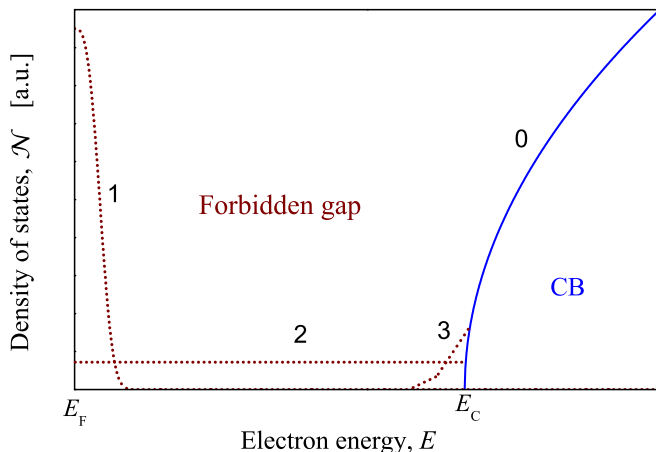


FIG. 7. (Color online) Schematic behavior of the density of empty electronic states  $\mathcal{N}(E)$ . Curve 0 corresponds to the CB density, while curves 1 and 2 illustrate cases 1 and 2 for the localized states in the forbidden gap, considered in the text. Line 3 illustrates the tail of localized states near the bottom of the CB.

For  $\varphi \neq 0$ , it is necessary to replace  $E$  with  $E - e\varphi(z)$  in the argument of  $\mathcal{N}$  to account for the  $\varphi$ -induced energy shifts. Integrating  $-e\mathcal{N}(E - e\varphi)$  over  $E$  up to  $E_F$  and subtracting the background density,  $-e \int_{-\infty}^{E_F} \mathcal{N}(E) dE$ , we arrive at the expression for the charge density of compensating electrons:

$$\rho = -e \int_0^{e\varphi} \mathcal{N}(E_F + E') dE'. \quad (22)$$

It is a generalization of the TF dependence  $\rho(\varphi)$  given by Eq. (6).

For a conduction band (CB) with the edge  $E_C$  and the parabolic dispersion law, we have  $\mathcal{N}(E) = (2m_e)^{3/2} (E - E_C)^{1/2} / 2\pi^2 \hbar^3$  for  $E > E_C$  and zero for  $E < E_C$ , as illustrated by curve 0 in Fig. 7. Generalizations of the band section of  $\mathcal{N}(E)$  for anisotropic and/or nonparabolic dispersion laws of electrons are available [40].

Within the energy range  $E_F \leq E \leq E_C$ , the function  $\mathcal{N}(E)$  is nonzero only due to localized states. Its shape incorporates a great deal of information about the energy distribution of empty traps. The total empty-trap concentration  $N_t = \int_{E_F}^{E_C} \mathcal{N}(E) dE$  is one of the simplest characteristics. Another useful characteristic is the density of states at the Fermi level  $\mathcal{N}(E_F)$ ; generally, it is nonzero.

Let  $\varphi(z)$  be the CDW potential profile. As follows from Eq. (22), the CB electrons contribute to  $\rho(z)$  only within the spatial region where  $e\varphi(z) > \Delta_C = E_C - E_F$ . Outside this region, the charge density would be zero in the absence of localized carriers leading to a linear growth of  $\varphi(z)$  with increasing  $|z|$ . Accounting for localized carriers changes the situation. The charge density  $\rho(\varphi) \neq 0$  in the whole range of  $\varphi(z)$  providing decay of the potential far away from the wall.

Details of the decay of  $\varphi(z)$  depend on the shape of  $\mathcal{N}(E)$  in the forbidden gap. One of the most playable shapes is Gaussian density of states centered at the Fermi level,

$$\mathcal{N} = \frac{2N_t}{\sqrt{\pi} \gamma} \exp \left[ -\frac{(E - E_F)^2}{\gamma^2} \right], \quad (23)$$

where  $\gamma$  is the energy-width parameter; see also line 1 in Fig. 7. The empty and filled-trap concentrations are the same here and equal to  $N_t$ . At  $\varphi = 0$  the electron charge density  $-eN_t$  is fully compensated by a positive background. For  $\gamma \rightarrow 0$ , the Gaussian shape can be approximated by the Dirac  $\delta$  function,  $\mathcal{N}(E) \simeq N_t \delta(E - E_F)$ . This case is relevant to the model of doped semiconductor. Another simple case is a constant density of states,  $\mathcal{N}(E) = N_t / \Delta_C$ ; see curve 2 in Fig. 7. Often the band section of  $\mathcal{N}(E)$ , shown by curve 0 in the same figure, continuously turns into a tail of localized states [41], shown schematically by dotted line 3.

The general scheme for calculation of the profiles  $\varphi(z)$ ,  $P(z)$ , and  $\rho(z)$  within the formalism of the density of electronic states is as follows. First, using Eq. (22) and any particular model for  $\mathcal{N}(E)$ , we calculate analytically the charge density  $\rho(\varphi)$  and the integral  $\int_0^\varphi \rho(\varphi') d\varphi'$ . Next, using the conservation law (3) we express algebraically  $p = P/P_0$  and  $1 - p^2$  with  $\varphi$ . Substituting these expressions into Eq. (1), we arrive at an ordinary first-order differential equation for  $\varphi$ . This equation can be integrated analytically or numerically to get  $\varphi(z)$  and, consequently,  $p(z)$  and  $\rho(z)$ .

Note that the value  $\varphi_{\max} = \varphi(0)$ , which is an important CDW characteristic, can be calculated even more easily: Since the maximum potential occurs at the head-to-head wall center, it is sufficient to set  $P = 0$  in Eq. (3) and take into account Eq. (22); see also Sec. IV C.

## B. Core and tails of CDW

Let us consider the structure of CDWs within the above formalism of the density of electronic states for sufficiently small values of the trap concentration.

We start from particular examples using the representative values of  $P_0$ ,  $|\alpha|$ , and  $m_e$  given by Eq. (15), the energy difference  $\Delta_C = E_C - E_F = 1$  eV, and Eq. (23) for  $\mathcal{N}(E)$  with  $\gamma \ll \Delta_C$ .

Lines 1 and 2 in Fig. 8(a) show the profile  $E_C - e\varphi(z)$  for  $N_t = 10^{17}$  and  $10^{18}$  cm $^{-3}$ , respectively. It consists of a narrow *core* part lying below  $E_F$  and a wide *tail* part above  $E_F$ . The same lines in Fig. 8(b) show the cores in more detail. Apart from a close vicinity of  $E_F$ , lines 1 and 2 coincide with each other and also with the function  $E_F - e\varphi(z)$ , where  $\varphi(z)$  is the TF profile of Sec. III C. The width and depth of the core,  $w$  and  $E_F - e\varphi(0)$ , respectively, coincide with the corresponding parameters of the TF model. The *tail* part possesses a much larger spatial scale  $\ell$ , and this scale substantially depends on  $N_t$ . For lines 1 and 2, the ratio  $2\ell/w$  is as large as  $\simeq 132$  and 44. The energy span of the tail is  $\Delta_C$ . The screening charge is predominantly concentrated in the core; the profile  $P(z)$  coincides here with the TF polarization profile.

Now we proceed to a more general description of the CDW structure. The properties of the tails admit a simple analytical description predicting important features. First of all, we obtain a general equation for  $\varphi$  in the range  $|z| \gtrsim (1 - 2)w$ , where  $P(z)$  is already close to  $P_0$  or  $-P_0$ . Setting  $P = \pm P_0 + \delta P$ , we get from Eqs. (1) and (2) in the linear approximation in  $\delta P$ :

$$\frac{d^2\varphi}{dz^2} + 2|\alpha|\rho(\varphi) = 0. \quad (24)$$

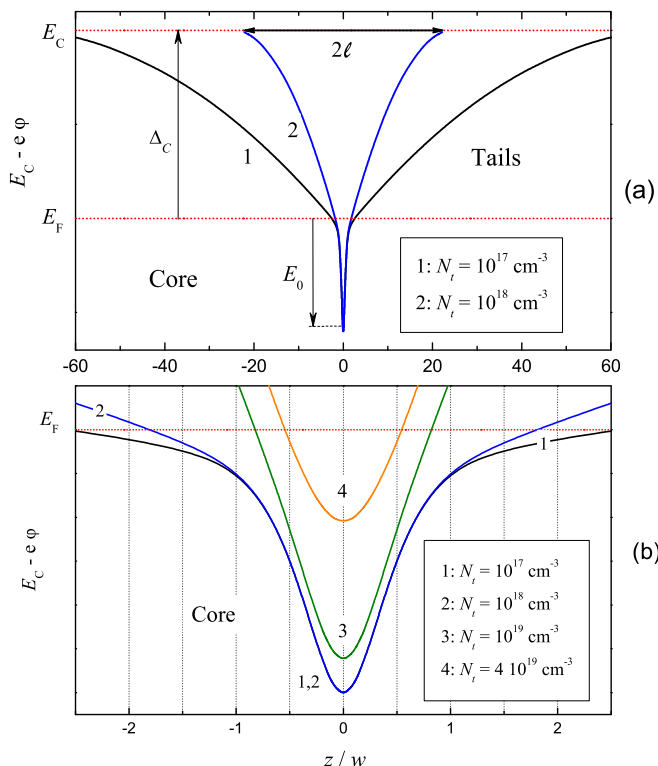


FIG. 8. (Color online) The CB edge  $E_C - e\varphi(z)$  versus  $z/w$  for  $\Delta_C = 1$  eV, the Gaussian density of localized states, and different values of  $N_t$ . Curves 1 and 2 in (a) show the core and tails for  $N_t = 10^{17}$  and  $10^{18}$   $\text{cm}^{-3}$ , respectively;  $\ell$  is the tail length. Panel (b) shows in detail the effect of  $N_t$  on the core.

This equation is nonlinear in the general case. Next, we indicate that the asymptotic decay of  $\varphi(z)$  for  $|z| \gg w$  is fully determined by the behavior of  $\mathcal{N}(E)$  near the Fermi level. Since  $\mathcal{N}(E_F) \neq 0$ , we have  $\rho \simeq -e^2 \mathcal{N}(E_F) \varphi$  for  $\varphi \rightarrow 0$  from Eq. (22). Equation (24) gives here an exponential decay  $\varphi \propto \exp(\mp qz)$  with the decay constant

$$q = e\sqrt{2|\alpha|\mathcal{N}(E_F)}. \quad (25)$$

The same decay law is inherent indeed in  $\delta P(z)$ . The smaller are  $\mathcal{N}(E_F)$  and  $|\alpha|$ , the weaker is the decay.

Let us consider particular analytical solutions for the tails. In the case of Gaussian density of states given by Eq. (23), the charge density can be approximated by  $\rho \simeq -eN_t$  for  $\gamma \ll e\varphi < \Delta_C$ . Here we have from Eq. (24)

$$e\varphi = \Delta_C (|z|/\ell - 1)^2, \quad (26)$$

with the tail length

$$\ell = \sqrt{\Delta_C/e^2|\alpha|N_t}. \quad (27)$$

The potential turns to zero at  $z = \pm\ell$  according to Eq. (26). In reality, this relation breaks for  $e\varphi \lesssim \gamma$ , and the quadratic decay turns to a quick exponential one. The found solution for  $\varphi$  corresponds to Fig. 8(a).

In the case of constant density of states in the forbidden gap,  $\mathcal{N}(E) = N_t/\Delta_C$ , we have  $\rho = -e^2 N_t \varphi/\Delta_C$ . The shape of the tail is expressed here by

$$e\varphi = \Delta_C \exp(-\sqrt{2}|z|/\ell), \quad (28)$$

where  $\ell$  is given again by Eq. (27) and represents the half-width of the potential profile. For the same value of  $\ell$ , the tail is substantially broader here compared to that presented in Fig. 8(a).

Dependence of  $\ell$  on the key parameters is clear from Eq. (27): It decreases gradually with decreasing  $\Delta_C = E_C - E_F$  and increasing  $N_t$ . To make a numerical estimate, we set  $N_t = 10^{17}$   $\text{cm}^{-3}$ , which is representative for undoped ferroelectrics. Using the former values of  $|\alpha|$  and  $\Delta_C$ , we obtain  $\ell \approx 1$   $\mu\text{m}$ . This is indeed much larger than the wall width  $w$ , indicating a pronounced two-scale screening behavior of the wall.

Next we estimate how small is the quantity  $1 - |p(z_s)|$  at the points  $z_s$  separating the core and tails and satisfying  $e\varphi(z_s) = \Delta_C$ ; see also Fig. 8. It is fully determined by the properties of localized electrons and can be easily calculated from Eqs. (3) and (22) for any particular model of  $\mathcal{N}(E)$ . For the Gaussian density of states with the width  $\gamma \ll \Delta_C$  [see Eq. (23)] we have

$$1 - |p(z_s)| \simeq \sqrt{N_t \Delta_C / |\alpha| P_0^2}. \quad (29)$$

For  $N_t = 10^{17}$   $\text{cm}^{-3}$  and parameters (15), we obtain  $1 - |p(z_s)| \simeq 0.05$ . In the case of constant density of states,  $\mathcal{N}(E) = N_t/\Delta_C$ , we have a  $\sqrt{2}$  times smaller value of  $1 - |p(z_s)|$ .

Transfer to the case of tail-to-tail walls, where the screening species are holes, presents no difficulties. It is necessary to replace  $\Delta_C$  with  $\Delta_V = E_F - E_V$  in Eq. (27) for  $\ell$ , to change the sign of  $\varphi$ , and to consider  $N_t$  as the filled-trap concentration. The core of the wall in Fig. 8 would lie here above  $E_F$ , and the valence band (VB) edge  $E_V - e\varphi(z)$  would tend to  $E_V$  with increasing  $|z|/\ell$ .

Until now we dealt with rather small values of the trap concentration. Lines 3 and 4 in Fig. 8(b) illustrate what happens with increasing  $N_t$ . For  $N_t = 10^{19}$   $\text{cm}^{-3}$ , the core is already noticeably distorted, and for  $N_t = 4 \times 10^{19}$   $\text{cm}^{-3}$  the TF screening regime greatly fails.

### C. Screening by localized electrons

An entirely different situation occurs when the concentration of localized levels in the forbidden gap is large enough. In this case, which can be realized in heavily doped crystals, the whole screening is due to redistribution of electrons among the localized states. Here the band carriers are of no importance and adjustment of the band edges to the Fermi level is absent. Only a single spatial scale—the wall width—is present in this case.

Let us employ again the Gaussian shape of  $\mathcal{N}(E)$  given by Eq. (23). For  $\varphi \neq 0$ , we have from Eq. (22) for the charge density of compensating electrons,

$$\rho = -eN_t \text{Erf}(e\varphi/\gamma), \quad (30)$$

where  $\text{Erf}(x) = (2/\sqrt{\pi}) \int_0^x \exp(-y^2) dy$  is the error function. Using next Eq. (3), we express  $p^2 = P^2/P_0^2$  by  $\varphi$ ,

$$p^2 = 1 - S(e\varphi/\gamma)/\sqrt{g}, \quad (31)$$

where  $g = |\alpha|P_0^2/4\gamma N_t$  is a dimensionless parameter and

$$S^2(x) = \int_0^x \text{Erf}(x') dx' \equiv x \text{Erf}(x) - (1 - e^{-x^2})/\sqrt{\pi}.$$

The maximum value of  $\varphi(z)$  occurs at the wall center where  $p = 0$ . Thus, we have an explicit relation for  $\varphi(0)$ ,

$$S^2[e\varphi(0)/\gamma] = g. \quad (32)$$

In the most important case of narrow peak of  $\mathcal{N}(E)$ , when the potential well depth  $e\varphi(0) \gg \gamma$ , we have

$$e\varphi(0) \simeq g\gamma = |\alpha|P_0^2/4N_t \quad (33)$$

and  $g \gg 1$ . The well depth does not depend here on the width parameter  $\gamma$ .

If  $e\varphi(0) < \Delta_C$ , then the CB edge is above the Fermi level, so that the TF screening is not involved. Setting  $\Delta_C = 1$  eV,  $|\alpha| = 0.01$ , and  $P_0 = 30 \mu\text{C}/\text{cm}^2$ , we have the inequality  $N_t > 5 \times 10^{19} \text{cm}^{-3}$ . It can be realized in heavily doped ferroelectrics. For substantially smaller values of  $N_t$  we return to the TF screening regime.

Let us consider the spatial structure of the wall. Combining Eqs. (1) and (31), we obtain

$$\int_{e\varphi/\gamma}^{e\varphi(0)/\gamma} \frac{\sqrt{g} dx}{S(x)[1 - S(x)/\sqrt{g}]^{1/2}} = \frac{e|\alpha|P_0 z}{\gamma}. \quad (34)$$

It gives the dependencies  $\varphi(z)$  and  $S[e\varphi(z)/\gamma]$ . Employing again Eq. (31) for  $p^2$ , we get the profile  $p(z)$ .

The expressions for  $\varphi(z)$  and  $p(z)$  can be strongly simplified if we restrict ourselves to the region where  $e\varphi(z) \gg \gamma$ , i.e., exclude the far tail areas. Here we have  $S(x) = \sqrt{x}$  with a high accuracy and, consequently,

$$\frac{\varphi(z)}{\varphi(0)} = \left(1 - \frac{z^2}{z_0^2}\right)^2, \quad \frac{P}{P_0} = -\frac{z}{z_0}, \quad (35)$$

where  $z_0 = P_0/eN_t$  is a new characteristic spatial scale representing the wall width. It is well above 1 nm for typical values of  $P_0$ . For  $P_0 = 30 \mu\text{C}/\text{cm}^2$  and  $N_t \approx 10^{20} \text{cm}^{-3}$ , the wall width can be estimated as  $z_0 \approx 18$  nm.

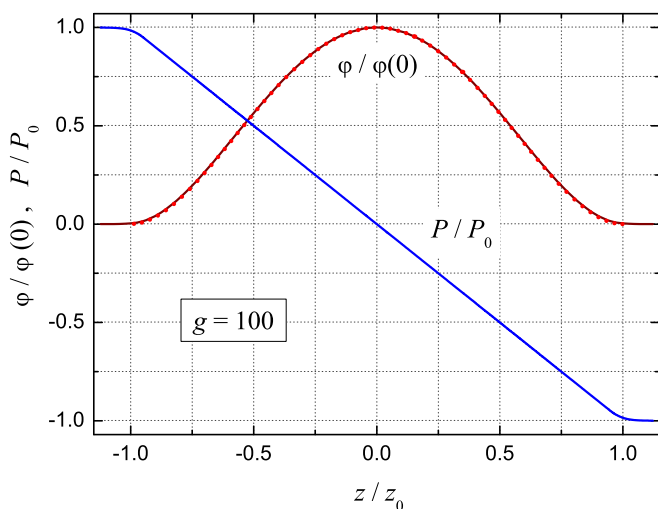


FIG. 9. (Color online) Dependencies  $\varphi(z)/\varphi(0)$  and  $P(z)/P_0$  for  $g = 100$  (solid lines). The dotted line corresponds to Eq. (35) for  $\varphi$ .

The solid lines in Fig. 9 show the spatial profiles  $\varphi(z)$  and  $p(z)$  for  $g = e\varphi(0)/\gamma = 100$ , which correspond a narrow distribution of the localized states near the Fermi level. The dotted line corresponds to the above approximation for  $\varphi(z)$ . One sees that the tails are very weak, so that the use of Eqs. (35) is well justified. With decreasing  $g$ , the tails become gradually more pronounced.

## D. Domain wall energies

### 1. General relations

With the known dependencies  $P(z)$ ,  $\varphi(z)$ , and  $\rho(z)$ , we are able to evaluate the domain-wall formation energy  $W$ , which is the difference between the energies of the crystal with and without the wall. For dielectrics, the starting point of consideration would be the expression  $-(d\varphi/dz)dD/4\pi$  for the differential of the energy density [36]. Being supplemented by the equation of state (1), it gives two known contributions to  $W$ :

$$W_1 = \frac{\varepsilon_b}{8\pi} \int \left(\frac{d\varphi}{dz}\right)^2 dz, \quad W_2 = \frac{|\alpha|P_0^2}{4} \int (1 - p^2)^2 dz. \quad (36)$$

The first contribution is the electrostatic energy of the total (bound + free) charge distribution. It is negligible compared to the second contribution, the lattice energy. The corresponding smallness parameter is  $\varepsilon_b/\varepsilon_f = |\alpha|\varepsilon_b/2\pi \ll 1$ .

However, the above basic expression for the energy density differential does not account for the fact that the charge density  $\rho$  is a function of  $\varphi$  such that  $\rho(0) = 0$ . This leads to an additional contribution to  $W$ . Employing the general expression for the electron energy density  $\int_{-\infty}^{E_F} E \mathcal{N}(E + e\varphi) dE$  and setting aside the potential energy of electrons (already included in  $W_1$ ), we obtain the additional contribution

$$W_3 = \iint_0^{e\varphi} E' \mathcal{N}(E_F + E') dE' dz. \quad (37)$$

This expression covers uniformly the cases of localized and delocalized (band) carriers. The contribution  $W_3$  can be regarded as excess energy of screening electrons. It accounts for redistribution of electrons caused by the  $\varphi$ -induced shifts of the energy levels. Note that small energy shifts caused by the polarization changes and elastic strains can, if necessary, also be included in  $W_3$ .

As follows from Eq. (37), the differential of the excess energy density is  $-\varphi d\rho \equiv -d(\rho\varphi) + \rho d\varphi$ . Correspondingly, the differential of the total energy density is given by  $-(d\varphi/dz)dD/4\pi - \varphi d\rho$ . This relation generalizes the known thermodynamic relation for dielectrics [36].

Next, using the above relation for  $-\varphi d\rho$  we represent the excess energy density as  $-\rho\varphi + \int_0^\varphi \rho(\varphi') d\varphi'$ . The integral term in this relation can be expressed by the lattice energy density using Eq. (3). After that, we get readily for the total wall energy

$$W \simeq W_2 + W_3 = - \int \rho(z)\varphi(z) dz. \quad (38)$$

Whereas both contributions  $W_{2,3}$  are of nonelectrostatic origin, their sum is nothing but the sign-inverted potential energy of the compensating electrons in the potential  $\varphi(z)$ . This quantity

is indeed positive. Furthermore, it is sensitive to both short- and long-range features of the potential profile.

## 2. Particular results

In the case of TF screening, the main contribution to  $W$  comes from the core of the wall, where  $e\varphi \simeq \Delta_C + e\varphi_{\text{core}}(z)$  and  $\varphi_{\text{core}}$  is as in Sec. III. Using Eq. (38), we obtain in the head-to-head case,

$$W_e \simeq (\Delta_C + 0.7|E_0|) \times 2P_0/e, \quad (39)$$

where  $|E_0| \simeq e\varphi_{\text{core}}(0)$  represents the binding energy of electrons [see Eq. (20)] and the number 0.7 accounts for the shape of the TF core. The second factor in this relation is the bound charge density. The limit  $\Delta_C \equiv E_C - E_F \rightarrow 0$  corresponds to the case of 1D atom. To obtain the energy  $W_h$  of the tail-to-tail wall, it is sufficient to replace here  $\Delta_C$  by  $\Delta_V = E_F - E_V$  and to treat  $|E_0|$  as the binding energy of holes.

If the binding energies are substantially smaller than the forbidden gap  $E_g$ , we have for the sum  $W_e + W_h \simeq E_g \times 2|P_0|/e$ . This corresponds to the result of [28].

In the case of wall screening by localized carriers, we have using Eqs. (30), (35), and (38):

$$W_e \simeq \frac{8}{15} \times e\varphi(0) \times 2P_0/e \simeq \frac{4|\alpha|P_0^3}{eN_t}. \quad (40)$$

Since  $e\varphi(0) < \Delta_C$ , it is smaller than the value given by Eq. (39). To get an expression for  $W_h$ , one should treat  $N_t$  as the filled-trap concentration.

Strictly speaking, the use of Eq. (38) for a single CDW is not quite correct because the bound charges at the crystal faces are different in the initial and final states; see Fig. 1(a). Consideration of wall pairs is correct in this sense. However, owing to the locality of the wall properties, the total energy can be presented as the sum  $W_e + W_h$ .

## V. SUMMARY

The results of this paper break up into two parts supplementing each other. In the *first part*, we give a new view on the properties of CDWs in ferroelectrics, including 180° and 90° walls. The wall is treated as a neutral 1D multielectron quantum system, where the electron charge density  $\rho$  is not generally a function of the electrostatic potential  $\varphi$ . On the contrary, the potential  $\varphi(z)$  harbors a set of localized electronic states with energies  $E_j$  and wave functions  $\Psi_j(z)$ , so that the charge density  $\rho(z)$  is a result of filling these states with electrons which are confined in  $z$  and free in  $x, y$ . The key physical quantities— $P(z)$ ,  $\varphi(z)$ ,  $\Psi_j(z)$ ,  $E_j$ , and the occupation numbers of the states—are found self-consistently. The basis for our analysis is the Hartree and TF methods and the Landau theory of the ferroelectric state. A close analogy for our quantum system is neutral multielectron atoms.

Despite an apparent complexity, our quantum system shows a fairly simple behavior. This system is controlled by a single dimensionless parameter  $Q$  combining the ferroelectric characteristics and the effective electron mass. It ranges from  $Q \sim 1$  to  $\sim 10^2$  (ordinary ferroelectrics with  $P_0 \sim 30 \mu\text{C}/\text{cm}^2$  and  $|\alpha| = 2\pi/\varepsilon_f \sim 10^{-2}$ ). Also, it controls the number of

localized levels in the wall, the binding energies of electrons, and the CDW width. The range  $0 < Q \lesssim 4$  is covered analytically and numerically with the Hartree method. Here the number of localized states ranges from 1 to 4, the binding energies are  $\sim 0.1$  eV, and the wall widths are  $\sim 1$  nm. Within this range, we have a nice, without any gaps, convergence to the quasiclassical TF pattern. On the upper end of the  $Q$  range, the number of levels is  $\sim 15$ , the binding energies approach  $\sim 1$  eV, and the wall widths are  $\sim 10$  nm. Large binding energies indicate weakness of the thermal effects and pronounced discreteness of the energy spectrum implies the presence of IR spectroscopic effects. For  $Q \gg 1$ , we have full agreement with [28] with regard to the polarization profile.

The above numerical estimates have to be modified for the case of 90° CDWs in trigonal BaTiO<sub>3</sub> [6]. Because of a strong dielectric anisotropy, the effective coefficients  $\alpha$  and  $\beta$  acquire here, compared to Eq. (15), an additional smallness factor  $\approx 1/15$  [37]. This results in an increase of the wall thickness by a factor of  $\approx 5$  and a decrease of the electron binding energy by a factor of  $\approx 4$ .

In the *second part*, we consider what happens when our quantum system is embedded into a real solid-state environment. This consideration is based on the formalism of the density of electronic states. It accounts for recharging of filled and empty localized states (traps) with the energies in the forbidden gap lying below and above the Fermi level  $E_F$ . This recharging was never considered before as applied to domain walls. Its impact is crucial. The electrostatic potential  $\varphi(z)$  acquires the property of *locality*: It decays far away from an individual CDW, so that the wall becomes electrically uncoupled from the crystal faces and neighboring walls.

The spatial structure of a CDW depends on the trap concentration  $N_t$ . If this concentration is not very high,  $N_t = (10^{17} - 10^{18}) \text{ cm}^{-3}$ , the wall shows a pronounced two-scale behavior; it consists of a short-range core and long-range tails. The core obeys the relations of the *first part*. In the tail regions, the potential  $\varphi(z)$  changes slowly and strongly in such a way to adjust the band edges (CB or VB) to the Fermi level near the core and *disappear* far from the wall. The tail length  $\ell$  lies in the  $\mu\text{m}$  range. For the trap concentrations  $N_t$  well above  $10^{19} \text{ cm}^{-3}$ , the results of the *first part* become unapplicable. Here the wall screening is fully due to the localized charge carriers and the separation into core and tails is absent. At  $N_t \approx 10^{20} \text{ cm}^{-3}$ , the CDW thickness for ordinary ferroelectrics can be estimated as  $w \approx 20$  nm.

The impact of trap recharging concerns also the formation energy of CDWs. Using formalism of the density of electronic states, we have generalized the known thermodynamic relation for the energy of dielectric to include the contribution of compensating electrons. With this generalization, we have derived simple relations for the wall energies. In the overlap regions, they agree with the relations of [28].

## ACKNOWLEDGMENTS

This project was supported by the Swiss National Science Foundation, Grant No. 200020-155887, by the government of the Russian Federation, Grant No. 2012-220-03-434, and by the Russian Academy of Sciences via the Presidium Program No. 1.

- [1] A. Ohtomo and H. Y. Hwang, *Nature (London)* **427**, 423 (2004).
- [2] S. Thiel, G. Hammerl, A. Schmehl, C. W. Schneider, and J. Mannhart, *Science* **313**, 1942 (2006).
- [3] J. Seidel, L. W. Martin, Q. He, Q. Zhan, Y.-H. Chu, A. Rother, M. E. Hawkrigde, P. Maksymovych, P. Yu, M. Gajek, N. Balke, S. V. Kalinin, S. Gemming, F. Wang, G. Catalan, J. F. Scott, N. A. Spaldin, J. Orenstein, and R. Ramesh, *Nat. Mater.* **8**, 229 (2009).
- [4] P. Maksymovych, A. N. Morozovska, P. Yu, E. A. Eliseev, Y. H. Chu, R. Ramesh, A. P. Baddorf, and S. V. Kalinin, *Nano Lett.* **12**, 209 (2012).
- [5] D. Meier, J. Seidel, A. Cano, K. Delaney, Y. Kumagai, M. Mostovoy, N. A. Spladin, and R. Ramesh, *Nat. Mater.* **11**, 284 (2012).
- [6] T. Sluka, A. K. Tagantsev, P. Bednyakov, and N. Setter, *Nat. Commun.* **4**, 1808 (2013).
- [7] A. Crassous, T. Sluka, A. K. Tagantsev, and N. Setter, *Nat. Nanotechnol.* **10**, 614 (2015).
- [8] G. Catalan, J. Seidel, R. Ramesh, and J. F. Scott, *Rev. Mod. Phys.* **84**, 119 (2012).
- [9] Z. Surowiak, J. Dec, R. Skulski, E. G. Fesenko, V. G. Gavril'yatchenko, and A. F. Semenchov, *Ferroelectrics* **20**, 277 (1978).
- [10] C. A. Randall, D. J. Barber, and R. W. Whatmore, *J. Mater. Sci.* **22**, 925 (1987).
- [11] V. Y. Shur, E. L. Rumyantsev, and A. L. Subbotin, *Ferroelectrics* **140**, 305 (1993).
- [12] S. B. Lang, V. D. Kugel, and G. Rosenman, *Ferroelectrics* **157**, 69 (1994).
- [13] A. A. Grekov, A. A. Adonin, and N. P. Protsenko, *Ferroelectrics* **13**, 483 (1976).
- [14] C. L. Jia, S. B. Mi, K. Urban, I. Vrejoiu, M. Alexe, and D. Hesse, *Nat. Mater.* **7**, 57 (2008).
- [15] P. Gao, C. T. Nelson, J. R. Jokisaari, S. H. Baek, C. W. Bark, Y. Zhang, E. Wang, D. G. Schlom, C. B. Eom, and X. Pan, *Nat. Commun.* **2**, 591 (2011).
- [16] P. Gao, J. Britson, J. R. Jokisaari, C. T. Nelson, S. H. Baek, Y. Wang, C. B. Eom, L. Q. Chen, and X. Pan, *Nat. Commun.* **4**, 2791 (2013).
- [17] Y. L. Tang, Y. L. Zhu, Y. J. Wang, W. Y. Wang, Y. B. Xu, W. J. Ren, Z. D. Zhang, and X. L. Ma, *Sci. Rep.* **4**, 4115 (2014).
- [18] S. Wada, K. Yako, K. Yokoo, H. Kakemoto, and T. Tsurumi, *Ferroelectrics* **334**, 17 (2006).
- [19] P. S. Bednyakov, T. Sluka, A. K. Tagantsev, D. Damjanovic, and N. Setter, *Sci. Rep.* **5**, 15819 (2015).
- [20] M. Schroeder, A. Haussmann, A. Thiessen, E. Soergel, T. Woike, and L. M. Eng, *Adv. Funct. Mater.* **22**, 3936 (2012).
- [21] V. Y. Shur, I. S. Baturin, A. R. Akhmatkhanov, D. S. Chezganov, and A. A. Esin, *Appl. Phys. Lett.* **103**, 102905 (2013).
- [22] T. Kampfe, P. Reichenbach, M. Schroder, A. Haussmann, L. M. Eng, T. Woike, and E. Soergel, *Phys. Rev. B* **89**, 035314 (2014).
- [23] T. Choi, Y. Horibe, H. T. Yi, Y. J. Choi, W. Wu, and S. W. Cheong, *Nat. Mater.* **9**, 253 (2010).
- [24] W. Wu, Y. Horibe, N. Lee, S. W. Cheong, and J. R. Guest, *Phys. Rev. Lett.* **108**, 077203 (2012).
- [25] Y. S. Oh, X. Luo, F. T. Huang, Y. Wang, and S. W. Cheong, *Nat. Mater.* **14**, 407 (2015).
- [26] F. Kagawa, S. Horiuchi, N. Minami, S. Ishibashi, K. Kobayashi, R. Kumai, Y. Murakami, and Y. Tokura, *Nano Lett.* **14**, 239 (2014).
- [27] B. M. Vul, G. M. Guro, and I. Ivanchik, *Ferroelectrics* **6**, 29 (1973).
- [28] M. Y. Gureev, A. K. Tagantsev, and N. Setter, *Phys. Rev. B* **83**, 184104 (2011).
- [29] M. Y. Gureev, P. Mokry, A. K. Tagantsev, and N. Setter, *Phys. Rev. B* **86**, 104104 (2012).
- [30] T. Sluka, A. K. Tagantsev, D. Damjanovic, M. Gureev, and N. Setter, *Nat. Commun.* **3**, 748 (2012).
- [31] E. A. Eliseev, A. N. Morozovska, G. S. Svechnikov, V. Gopalan, and V. Y. Shur, *Phys. Rev. B* **83**, 235313 (2011).
- [32] Z. Li, H. Wu, and W. Cao, *J. Appl. Phys.* **111**, 024106 (2012).
- [33] Y. Zuo, Y. A. Genenko, and B.-Xi. Xu, *J. Appl. Phys.* **116**, 044109 (2014).
- [34] P. Ondrejko, P. Marton, M. Guennou, N. Setter, and J. Hlinka, *Phys. Rev. B* **88**, 024114 (2013).
- [35] L. D. Landau and E. M. Lifshitz, *Quantum Mechanics* (Pergamon Press, London, 1965).
- [36] L. D. Landau and E. M. Lifshitz, *Electrodynamics of Continuous Media* (Pergamon Press, London, 1960).
- [37] P. V. Yudin, M. Y. Gureev, T. Sluka, A. K. Tagantsev, and N. Setter, *Phys. Rev. B* **91**, 060102(R) (2015).
- [38] R. G. Parr and W. Yang, *Density-Functional Theory of atoms and Molecules* (Oxford University Press, Oxford, UK, 1989).
- [39] This estimate is rooted in numerous studies in the photorefractive area, where the effective trap concentration is one of the key parameters; see L. Solymar, D. Webb, and A. Grunnet-Jepsen, *The Physics and Applications of Photorefractive Materials* (Clarendon Press, Oxford, UK, 1996).
- [40] S. M. Sze, *Semiconductor Devices Physics and Technology* (Wiley, New York, 1985).
- [41] B. I. Shklovskii and A. L. Efros, *Electronic Properties of Doped Semiconductors* (Springer, New York, 1984).